Geological Quarterly, 2020, **64** (3): 692–710
DOI: http://dx.doi.org/10.7306/gq.1547

The dolomite problem: evidence from 3D modeling, XRD and geochemical data of Zechstein reefs (Upper Permian, Germany)

Wolfgang BLENDINGER[1, *]

[1] Technische Universität Clausthal, Department of Petroleum Geology, Leibnizstr. 10, D-38678 Clausthal-Zellerfeld, Germany

Blendinger, W., 2020. The dolomite problem: evidence from 3D modeling, XRD and geochemical data of Zechstein reefs (Upper Permian, Germany). Geological Quarterly, **64** (3): 692–710, doi: 10.7306/gq.1547

Three-dimensional modeling of the limestone and dolomite distribution in an Upper Permian (Zechstein) stromatolite-bryozoan reef, ~500 m in diameter and 35 m thick (77 borehole cores, 172 data points), shows that dolomite occurs as laterally and vertically discontinuous intervals. The prevailing mineral phases are near-stoichiometric dolomite and Mg-free calcite (370 XRD and 274 XRF analyses). Both ^{13}C and ^{18}O (526 analyses) show a spread of ~10‰ and co-vary with the mineralogy; the heaviest dolomite and calcite ^{13}C differ by ~1.5‰. Diagenetic modifications caused by flowing meteoric fluids could account for the observed "inverted J" trend of stable and the radiogenic signature of $^{87}Sr/^{86}Sr$ (23 analyses), but neither vertical nor horizontal gradients occur in the reef modeled. Because the dolomite geometries are incompatible with those predicted by fluid flow models, and the limestone-dolomite difference in ^{13}C overlaps estimates of isotope fractionation associated with Mg content, the dolomite studied was a depositional Very High Mg Calcite recrystallized to dolomite in a semi-closed diagenetic system rather than a Low Mg Calcite transformed by a dolomitization process. The isotope pattern suggests biogenic fractionation and/or loss of heavy stable C and O and light Sr isotopes during diagenesis.

Key words: Zechstein, dolomite, limestone, isotopes, 3D modeling, fluid flow.

INTRODUCTION

One of the paradigms in sedimentary geology is that dolomite is created by a fluid flow process which adds Mg^{2+} to a calcite precursor. This poses a major, unresolved, problem called the dolomite problem: many dolomites most likely formed under low temperature conditions (e.g., Warren, 2000; Machel, 2004), but dolomite cannot be synthesized at low temperatures (e.g., Usdowski, 1994). The dolomite problem persists because dolomite still has not been synthesized at low temperatures, in spite of attempts to detail dolomite formation, for instance by reactive flow modeling (e.g., Gabellone and Whitaker, 2016).

What has practically never been performed is a comparative study of ancient dolomite and equivalent limestone, although this was suggested in Purser et al. (1994) as a step necessary for a potential solution of the dolomite problem. This question is here approached from a 3D modeling, mineral phase analysis and geochemical perspective in a carbonate succession which is in part limestone, in part dolomite. This condition is met in Upper Permian Zechstein reefs in Germany. Three-dimensional modeling is performed with the aim of mapping dolomite bodies and reconciling the resulting geometries with fluid flow models. XRD analyses were performed to quantity the mineral phases and to allocate these to geochemical signatures. Geochemical analyses were performed to quantify the signals of and differences between limestone and dolomite. Abbreviations used in this paper are LMC for low magnesium calcite, HMC for high magnesium calcite, and VHMC for very high magnesium calcite. Calcite and limestone are used as synonyms.

REGIONAL SETTING AND PREVIOUS WORK

The reefs studied are located in the immediate vicinity of uplifted Variscan basement, an intensely folded succession of Precambrian to Lower Carboniferous sedimentary and igneous rocks (Fig. 1A). The Upper Permian reefs of Germany formed in the so-called southern Permian basin, a shelf area covering large parts of central and northern Europe (Fig. 1B). Most of the stratigraphic succession in the Permian basin consists of evaporites alternating with carbonate intervals, often several hundred metres thick, with a hydrocarbon source rock, the *Kupferschiefer*, near its base. The oldest Zechstein reefs more or less directly overlie the "Variscan unconformity" along the former basin margin and often overlie topographic highs of the folded Paleozoic. The reefs are typically structurally uncomplicated and flat-lying (Fig. 2), though are commonly slightly rotated due to post-Permian tectonic activity. By comparison with e.g. the Permian Basin of North America they are small, typically a few tens of metres thick and a few hundred metres to a few kilometres in length.

The Zechstein reefs are composed of limestone and dolomite (Smith, 1981; Reijers, 2012). The reefs are often land-locked, small shelves (e.g., Kerkmann, 1969), though the reefs

* E-mail: wolfgang.blendinger@tu-clausthal.de

Received: May 4, 2020; accepted: June 17, 2020; first published online: August 5, 2020

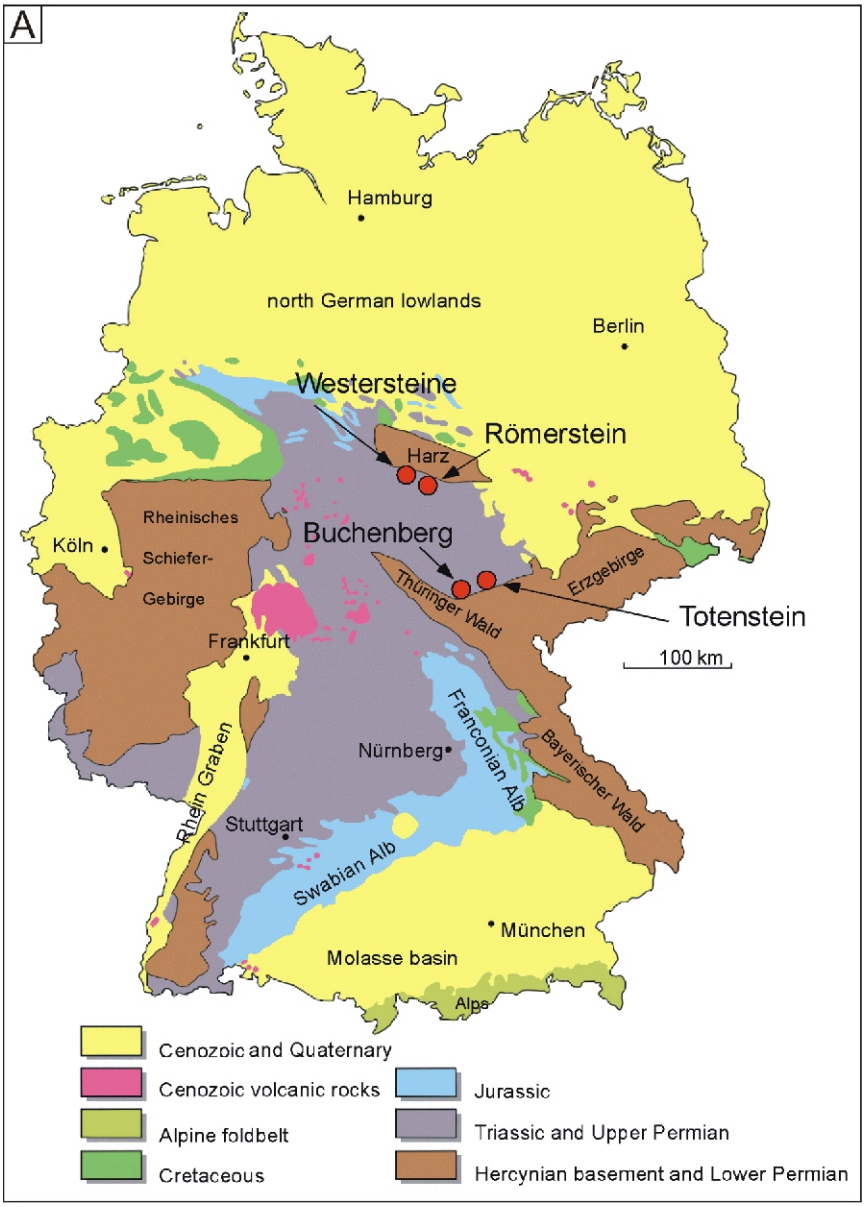

Fig. 1A – simplified geological map of Germany and location of the Zechstein reefs studied (red circles) at the periphery of Hercynian uplifts

studied developed as a result of isolated, local reef growth in nearshore environments and on intrabasin highs (Fig. 2A). Reef facies are subdivided into massive reef carbonate and, locally, reef flats consisting of discontinuously bedded carbonate, which forms the uppermost portions of the reef interior. Reef and reef flat consist of stromatolitic crusts and bryozoans, and locally contain abundant, originally aragonitic, cement. Reef dolomite has invariably been interpreted as the result of sinking brines dolomitizing the underlying carbonates, which is naturally the most plausible model in an overall evaporitic setting (e.g., Clark, 1980; Peryt et al., 2016). Four of these reefs were investigated (Figs. 1 and 2A). In decreasing amount of detail, these are the Buchenberg and Totenstein reefs in southern Thuringia, and the Römerstein and Westersteine reefs at the southern periphery of the Harz mountains in Lower Saxony. The former two reefs were described by Kerkmann (1969), whereas the latter two were investigated by Paul (1980). The Buchenberg reef (Figs. 2B and 3) has the highest data density for the purpose of the present study. It was quarried in the past century for limestone and has 77 fully cored exploration and appraisal boreholes allowing the reconstruction of the original reef shape and composition. The Totenstein reef is considered a classical locality showing a reef developing on an erosional high of Lower Paleozoic greywackes and shales, but it is comparatively poorly exposed. The reefs at the southern edge of the Harz mountains are now mostly covered by woodland and were spot sampled for comparison. Estimates of the maximum burial temperature, for instance from maturity data of the *Kupferschiefer*, are not available for the studied areas. Maximum overburden can be estimated at hundreds of metres, judging from the Permo-Mesozoic succession near the reefs studied.

The many facies studies of the Zechstein reefs contrast with the few geochemical studies. The dolomite isotope pattern of Polish subsurface reefs is relatively well known (Jasionowski et al., 2014; Peryt et al., 2016), but absent from the German out-

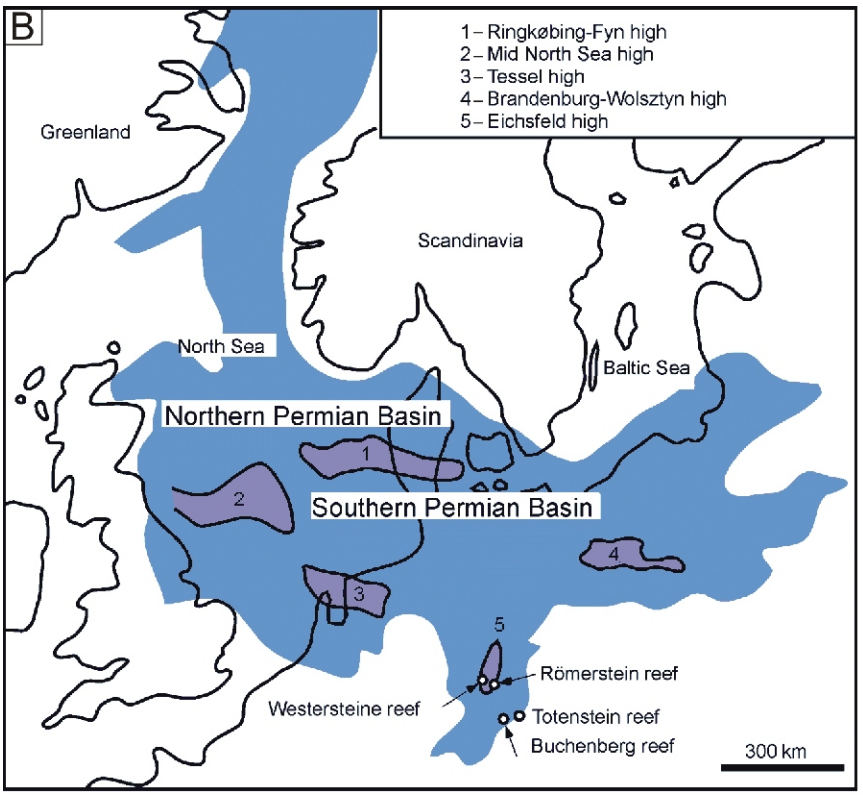

B – palaeogeography of the Permian basin (after Peryt et al., 2016) in central-northern Europe, showing the inferred marine area (blue) and intrabasinal highs (darker blue), and the approximate position of the reefs studied in the Permian sea

Totenstein and Buchenberg formed at the periphery, Westersteine and Römerstein are located on a small intra-basin high and were all primarily isolated reefs

crops. Stable isotope data of Zechstein carbonates mainly come from a stratigraphically somewhat higher interval, but do not include reef carbonate (Clark, 1980; Schönherr et al., 2018). Strontium isotope data are only available from the Polish subsurface reefs (Peryt et al., 2016). The data provided by these studies are from very different carbonate phases (matrix, fractures, and, particularly, dedolomite) but do not permit an answer to the question posed above.

ANALYTICAL METHODS

FIELDWORK

The four reefs were sampled (specimens of several cm^3 in size, Buchenberg 199, Totenstein 152, Römerstein 10, Westersteine 6) for geochemical and compositional phase analyses with the objective of quantifying the distribution of calcite and dolomite and of detecting possible trends in stable and radiogenic isotope values. XRD and isotope analyses were performed on the same samples, which, for the Buchenberg, were obtained along a ~10 m grid, which was only partly possible for reasons of topography. The other reefs were sampled in small stratigraphic sections or at random. Three hand specimens, measuring ~20 30 cm and referred to as A, B and C, were collected randomly, slabbed and polished for isotope and XRF analysis along regular grids, with grid width ranging for 1 cm to 4 cm. Carbonate-filled fracture orientation was logged on the pavements in the Buchenberg quarry (Fig. 4).

X-RAY DIFFRACTION (XRD) AND X-RAY FLUORESCENCE (XRF)

For the purpose of better quantifying the mineralogical database, X-ray diffractometry was carried out on 370 exposure samples (Buchenberg 199, Totenstein 152, Römerstein 10, Westersteine 3, and 6 samples from one hand specimen). For the X-ray phase analyses a *PhilipsPW1710* with Co or Cu K -radiation (1. nm; Ni filter, under 30 kV and 30 mA with a step increment of 0.004°) was used. Approximately 1 cm^3 of each sample was powdered to analytical fineness in a vibratory disc mill using a tungsten carbide grinding set. For the semi-quantitative determination of the content of different carbonates and the exact location of the dolomite and calcite d(104) peak in the samples, CaF_2 was added as internal standard in a ratio of 1:5. In order to achieve randomly oriented aggregates which allow comparison of relative intensities for a series of peaks, the powder was carefully scraped into the cavity of the aluminum holder and only gently pressed with a glass slide to counteract the tendency of particles to lie parallel to the glass surface. The evaluation was performed using the software program *Xpert High Score* (by Panalytical). Three hand specimens were slabbed, polished and analysed with a portable X-ray fluorescence analyzer *Niton XL3t* (by Analyticon) for Ca, Mg and Sr along a grid with a width of 1 cm, the other two along a 2 cm grid . A total of 274 measurements were carried out. In order to allow a correction for acid fractionation of ^{18}O of the hand specimens, the dolomite content was calculated with an empirically derived formula, based on the observation that pure calcite contains ~44% Ca, whereas pure dolomite contains ~25% Ca:

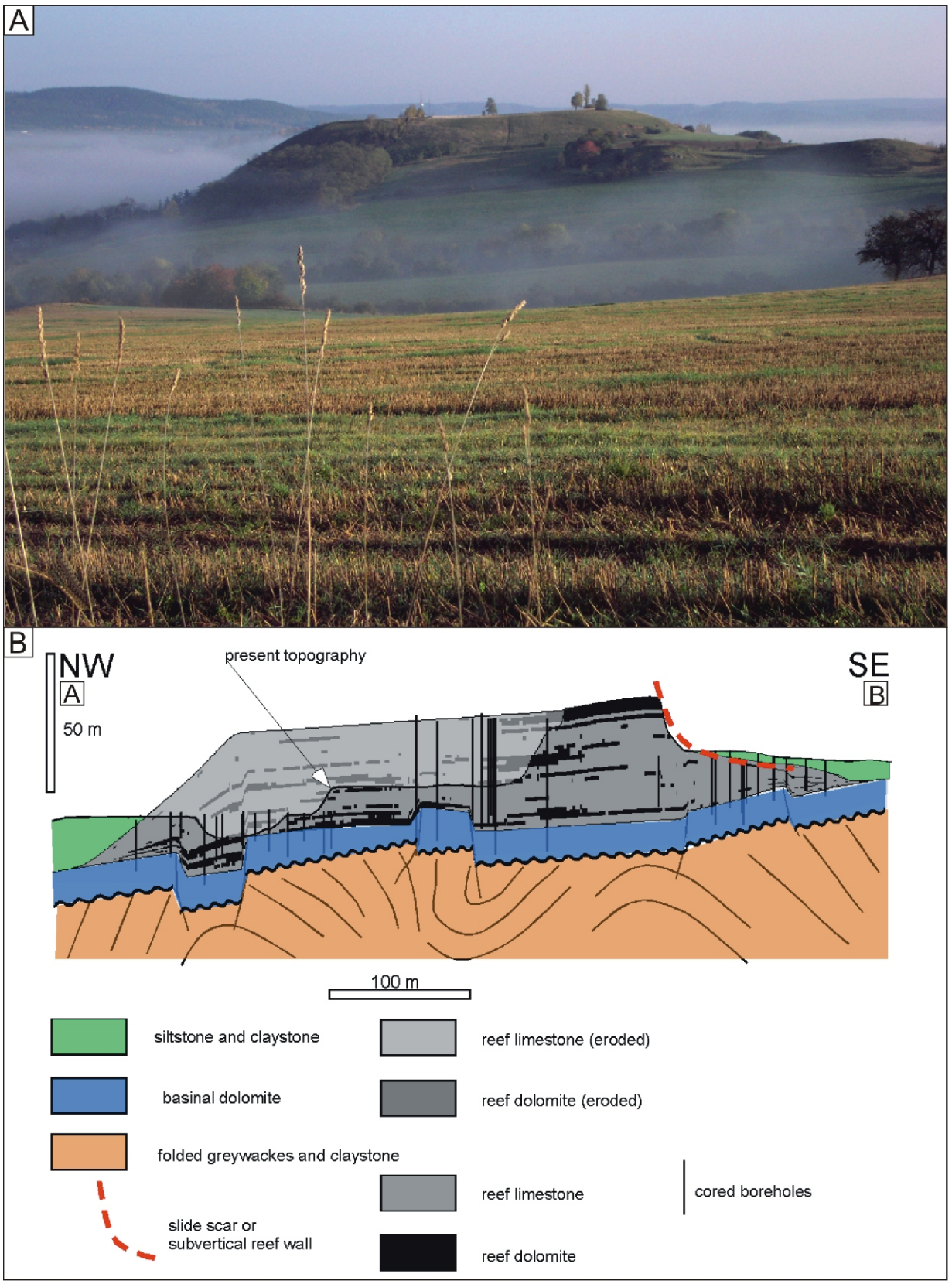

Fig. 2A – perfectly exhumed topography of a Thuringian reef (Schlechteberg reef, located ~0.5 km east of the Buchenberg) showing reef flat and reef flanks, exposed reef topography is ~30 m, structural dip is ~2°NW (to the left); B – cross-section of the Buchenberg reef (for location see Fig. 4), boreholes are projected from within 50 m distance of the cross-section, dolomite is black, limestone light grey, pale colours correspond to the quarried part, the section is 2x vertically exaggerated, the fold pattern of the strata below the unconformity is projected from a creek ~500 m west of the Buchenberg

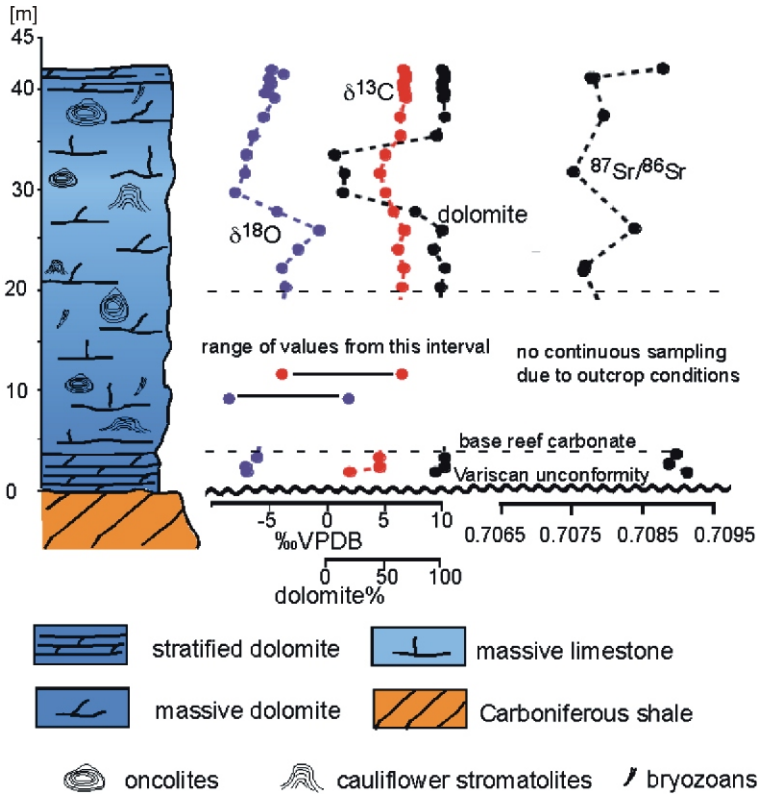

Fig. 3. Stratigraphic section of the Buchenberg reef showing lithology and continuously sampled section with the geochemical data logged in a vertical section of the Buchenberg reef

No continuous vertical section is exposed for the lower part of the reef; the data from directly above the Variscan unconformity are projected from the Totenstein reef

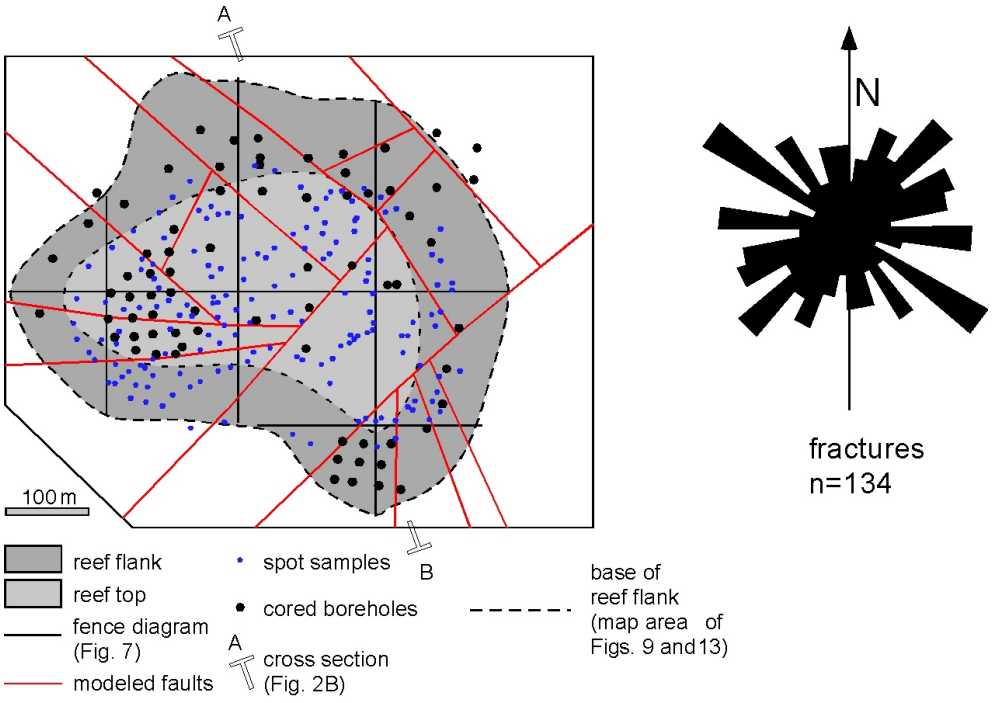

Fig. 4. Dimensions and constituents of the 3D model of the Buchenberg reef showing the location of the cross-section of Figure 2B, the fence diagram of Figure 7, and the outline of the maps of Figures 9 and 13

The rose diagram shows the orientation of carbonate-filled fractures on the pavements of the quarry

dolomite_percentage = (19/(44–Ca_%)*100 [1]

This determination of the dolomite content is not very accurate, because it assumes that all Ca and Mg are in carbonate, and may lead to a slight over- or under-correction of the dolomite ^{18}O. The maximum error is 1.1‰ and, because ^{18}O values are not interpreted to this level of uncertainty, this appears tolerable.

The point data from the Buchenberg outcrop and hand specimens were interpolated as 2D surfaces in *Petrel* using the isochore mapping algorithm, which is, in principle, a simple interpolation of values. Because the microprobe grid and stable isotope grid were shifted by 5 mm in sample A, the points at which isotope measurement was made were re-sampled in *Petrel* from the interpolated dolomite content surface at the location of the isotope samples. The raw data of the stable isotope and XRD measurements are in Appendix 1*, the XRF data from the hand specimens are in Appendix 2.

STABLE ISOTOPES

526 samples for stable isotopes of oxygen and carbon (365 dolomites, 161 limestones) were analysed at the Geozentrum Nordbayern, Erlangen and the Isotope unit of Göttingen University, respectively. 199 samples came from the Buchenberg reef, 145 from the Totenstein and 10 from the Römerstein reef. Three slabbed and polished surfaces of hand specimens from the Buchenberg were investigated, sample A with a 1 cm grid (142 samples), sample B with 4 cm grid (12 samples), and sample C with a 2 cm grid (19 samples). Sample material (0.5–1 g) was drilled with a 1 mm bit from fractured rock samples and slabbed surfaces, respectively, and reacted with 100% phosphoric acid at 70°C using a Gasbench II connected to a *ThermoFisher Delta V Plus* mass spectrometer. Reproducibility and accuracy was monitored by replicate analysis of laboratory standards calibrated by assigning ^{13}C values of +1.95‰ to NBS19 and –47.3‰ to IAEA-CO9 and ^{18}O values of –2.20‰ to NBS19 and –23.2‰ to NBS18. Reproducibility for ^{13}C and ^{18}O was ~±0.05‰. The ^{18}O data were corrected in the laboratories using the phosphoric acid fractionation factors given by Kim et al. (2007) and Rosenbaum and Sheppard (1986) and reported for calcite relative to the VPDB standard in the usual delta notation. Phosphoric acid fractionation of dolomitic samples (dolomite content determined by XRD) was corrected with the formula:

$$^{18}O\ (corr) = {}^{18}O\ (reported) - ((dolomite\%\ /100)*1.2) \quad [2]$$

Sr ISOTOPES AND CONCENTRATION

23 carbonate samples (9 from the Buchenberg, 14 from the Totenstein) were analysed for $^{87}Sr/^{86}Sr$ ratios at the Institute for Material Analysis and Science, Göttingen. Prior to digestion all samples were spiked with a tracer solution (Sr 4-AD) and dissolved in Teflon flasks by various steps of addition and evaporation of 2.5 N HCl until complete dissolution. The column procedure using Micro Bio-Spin Columns (Bio-Rad) with Sr-Resin-B (Triskem) was applied to separate Sr. The isotope measurements were made with a *ThermoFinnigan TIMS Triton TI*. Instrumental mass bias was corrected with $^{88}Sr/^{86}Sr$ of 0.1194 using an exponential law. Concentrations were calculated using the ID-TIMS technique. Within this study, the average value for NBS 987 (n = 9) is 0.71027 ±7 which is consistent with the long-term average $^{87}Sr/^{86}Sr$ value of the laboratory (0.71027 ±5, n = 466). Strontium concentrations were measured from hand specimens by XRF at 341 sample points from 3 slabbed and polished hand specimens and reported in increments of 15 ppm. The Isotope data are included in the Appendix 1.

3D MODELING

In order to quantify the amount and geometries of dolomite, the Buchenberg reef was modelled in three dimensions with the commercially available program *Petrel* (by Schlumberger), using borehole data and the point data resulting from field sampling (Fig. 4). The data of 77 borehole cores were transformed into digital well paths and logs with codes for the lithology ranging from 1 (dolomite) to 5 (limestone). These were loaded in *Petrel*, and, honouring the prevailing slight structural dip to the NW (cf. Fig. 2), the following surfaces were constructed: the reef top, the top of the basinal dolomite, and the top of the Variscan unconformity. It is not clear from the borehole data whether the unconformity is an irregular surface caused by pre-Zechstein erosion, or a faulted surface with displacements on a metre scale. It is, however, irrelevant for the present study which of the two options corresponds to reality. The fault option was preferred, and a fault model honoring the fracture measurements was constructed. The original topography of the reef top, now nearly completely removed by excavation, is well constrained by borehole data. The surfaces were used as input to subdivide a 3D grid measuring ~700(E–W) 570(N–S) m and a cell size of 2 2 m (x, y) into 30 layers in order to obtain a vertical resolution of ca. 1m in the reef interior, though with wedge shaped cells in the reef flanks. The reef model consists of 2.967.360 cells. The lithology codes from boreholes and spot samples were assigned to the grid cells penetrated by boreholes or corresponding to the spot sample locations, respectively. This “upscaling” step was followed by a modeling process, in which each cell of the reef obtained a lithology code, based on the upscaled codes, using the “Gaussian sequential simulation” in *Petrel*. This is, in principle, a simple interpolation between the upscaled cells, where the resulting bodies cannot crosscut each other or extend into neighbouring boreholes with different lithologies. For visualization, the lithology codes 4 and 5 were set to show “limestone”, whereas the codes 1 to 3 were set to show “dolomite”. Two facies maps were created, which show the average of the sum of cell properties in the vertical cell stack at each model point. For instance, if each of the 30 stacked cells had facies code 1, the average for all cells at this point of the result map is code 1 (30 1/30). The model cells above the present topography (i.e., those quarried or now eroded) were then removed, resulting in 933.051 cells remaining.

The quality assurance of the model was performed by quantifying the percentage of input data and comparing these with the upscaled model cells and the total volume of the entire model. For comparison with the 3D modeling results, the parameters of the Buchenberg 172 data points (lithology, stable isotopes) were interpolated in *Petrel* in 2D (x, y) in a separate step.

* Supplementary data associated with this article can be found, in the online version, at doi: 10.7306/gq.1547

RESULTS

REEF DOLOMITE AND LIMESTONE DISTRIBUTION

The reefs studied consist of tight to highly porous limestone and dolomite which is generally very friable in all reefs. The two lithologies are not easily distinguished in the field unless HCl is used. Stromatolitic fabric is generally easily recognizable and encompasses various forms, which range from small cauliflowers to nodules (Fig. 5A–C) with dimensions varying from centimetres to decimetres. The stromatolite layers show changes in porosity from completely tight, micritic portions to parts with an estimated 30% porosity both in calcitic and dolomitic parts (Fig. 5A). The spaces between individual nodules are open (Fig. 5A) and, when aligned parallel to stratification, often a decimetre long and a few centimetres high. Bryozoans are calcareous or dolomitic in dolomite, are common as fragments, but comparatively rare as complete specimens. They occur concentrated in local patches in the reef interior and in the uppermost reef layers (Fig. 3).

Thin sections show that dolomite and limestone preserve a clotted-peloidal, microcrystalline fabric (Fig. 5B–D), occasionally showing isolated dolomite rhombs in limestone and micron-sized, micritic tubes or brushes of possibly bacterial origin (Fig. 5E). In samples where dolomite co-occurs with calcite, dolomite crystals are generally corroded and occasionally partly replaced by calcite (Fig. 5E). The larger dolomite crystals show a turbid core with relics of the clotted-peloidal fabric surrounded by a clear rim, similar to what is observed in most ancient dolomites (Purser et al., 1994).

Primary pore spaces are lined by thin, isopachous rims of almost transparent calcite or dolomite crystals with euhedral to anhedral edges lacking evidence for corrosion (Fig. 5D). Blocky cements of coarser crystal size are very rare and occur mainly as fracture fills. Isolated quartz grains, rounded to subangular and of silt to sand size, are common but volumetrically unimportant with an estimated 1% maximum. These characteristics allow a classification as partly recrystallized limestone and microcrystalline dolomite with high residual primary and intercrystalline porosity, respectively. The paragenesis of minerals of the reefs studied was not quantified, but no evidence for high temperatures, such as saddle dolomite, was found.

The reefs are underlain by a few metres of thin, tight, bedded, yellowish dolomite, called herein the basinal facies, containing productid brachiopods and bivalves, that lies directly above the unconformity (Fig. 2B). Borehole data indicate that the basinal facies is locally absent from the central parts of the Buchenberg reef. Borehole core data show that the lateral equivalents of the reefs are (unexposed) varicoloured siltstone and claystone with thin sandstone interbeds (Fig. 2B). Core data also show that the southeastern corner of the Buchenberg shows a small area where these siltstones terminate against a nearly vertical cliff of the reef (Fig. 2B). This is either a slide scar or a primary reef wall.

THREE-DIMENSIONAL MODELING AND PARAMETER INTERPOLATION

The 3D model of the Buchenberg shows that the reef consists of ~35% dolomite (facies codes 1, 2 and 3) and ~65% limestone (facies codes 4 and 5). Dolomite is slightly underrepresented in the model as compared to the input borehole and point data (40.1 and 35.2%, respectively, Fig. 6). The underrepresentation is partly a consequence of the upscaling, partly due to the modeling algorithm of *Petrel*. Dolomite occurs generally as laterally discontinuous intervals surrounded by limestone. In the southwestern part of the reef, a larger dolomite body existed and extended to the reef top, which is now completely removed by quarrying (Fig. 7). The lateral extent of individual dolomite intervals does not exceed a few tens of metres, and none extend over the entire reef (Fig. 7). The average maps show a very patchy distribution of dolomite interpolated from the point data (Fig. 8) and a concentration of dolomite in the SW part of the reef (Fig. 9A, B).

XRD AND XRF

X-ray diffractograms show that, as expected, two mineral phases dominate the reef carbonates investigated (Fig. 10). The first is dolomite (Fig. 10C). This phase has well developed ordering peaks, whereas a d(104) peak shift is not observed, indicating that the dolomite is near stoichiometric.

The second phase is calcite (Fig. 10A, B). In most cases, calcite does not show a d(104) peak shift but corresponds to a Mg-free LMC. A few samples of the Römerstein reef do show a d(104) peak shift of calcite towards somewhat higher degrees of 2 theta indicating a $MgCO_3$ content of 2–4 mol%, but the calcite peak is broad, and ordering reflections are poorly developed (Fig. 10C). Otherwise, Römerstein and Westersteine are entirely of dolomite.

Very low (1–2%) quantities of quartz (Fig. 10A) are present in many samples. Similarly low quantities of gypsum occur in the Römerstein reef, but evaporites are below detection limit in all other samples. This is somewhat surprising in an overall evaporitic setting and the fact that evaporites are exposed within close distances (a few hundred metres) of the reefs studied except for the Totenstein.

X-ray diffraction indicates that most samples have a dolomite content of <20% and >80%, respectively. Intermediate values are comparatively rare and come mostly from XRF data from the hand specimens. Pure calcite or dolomite (0% of the other mineral phase) are rare, too. It is important to note that, based on these results, all intermediate values are a physical mixture of Mg-free calcite and near stoichiometric dolomite. This is no surprise in view of empirical stoichiometry data of ancient calcite and dolomite (e.g., Searl, 1994). The hand specimens document gradual changes in the Ca/Mg ratio and, therefore, dolomite (and isotope) content (Fig. 8).

STABLE ISOTOPES

The stable isotopes of dolomite (here defined as calcite content <50% as determined by XRD) range from 6.6 to –1.4‰ and –8.9 to 2.6‰ for ^{13}C and ^{18}O, respectively (Fig. 11A). Calcite (here defined as dolomite content <50%) ranges from 6.3 to –3.9‰ and –9.9 to 0.3‰ for ^{13}C and ^{18}O, respectively. The spread of 9–12 ‰ is observed in both limestone and dolomite ^{13}C and ^{18}O. The pattern is similar for the two extensively sampled reefs (Fig. 11B). The histograms (Fig. 12) show that most dolomite has ^{13}C values >6‰, whereas calcite has a bimodal distribution with a maximum between ~–3 and –4‰, and another between +3‰ and +4‰. The histograms for ^{18}O show a maximum between –1 and –2‰ for dolomite and –6 and –7‰ for calcite (Fig. 12). Both dolomite and calcite are defined by maximum ^{13}C values of ~6.5‰ and 5‰, respectively (Fig. 11C). Dolomite content *versus* stable isotopes (Fig. 11C) shows covariant trends with correlation coefficients of ~0.44 for ^{13}C *versus* dolomite percentage, and ~0.55 for ^{18}O *versus* dolomite percentage. The section sampled at the Buchenberg (Fig. 3) shows an irregular pattern and no vertical isotope or mineralogy trend.

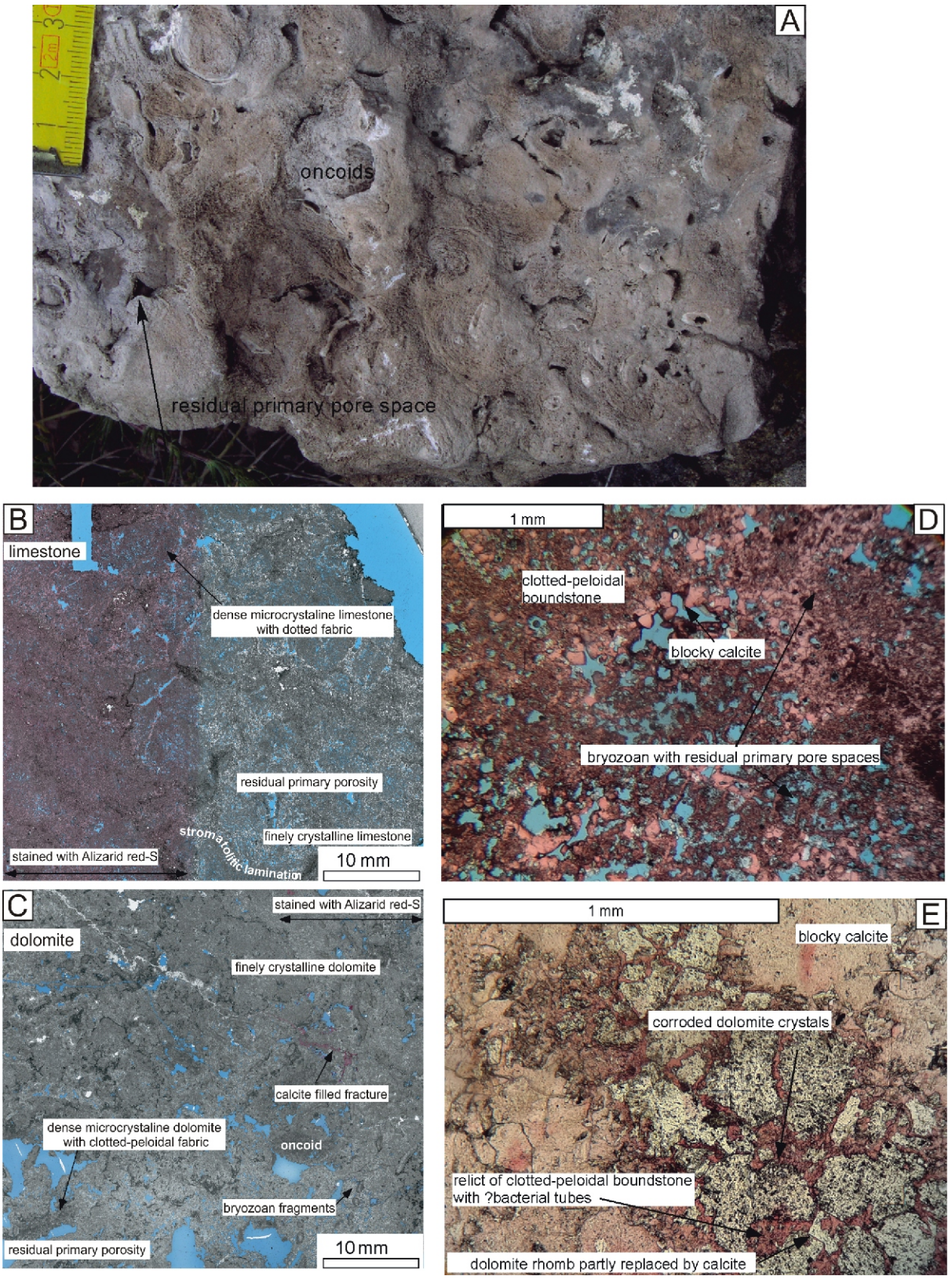

Fig. 5A – macroscopic reef fabric consists predominantly of stromatolitic carbonate, here in the form of large oncolitic nodules; scale bar in the centimetres; B – a thin section micrograph of limestone, blue dye-impregnated to show porosity, with tight (dark areas) and porous areas (blue) and stromatolitic lamination; C – thin section micrograph of a dolomite showing a fabric similar to that of the limestone of (A) but with common bryozoan fragments and large residual primary pore spaces; D, E – details of the paragenesis and are from blue dye-impregnated thin sections stained with Alizarin red-S: D – the gradual transition of the clotted-peloidal fabric into coarser blocky calcite lining residual primary pore spaces, E – dolomite crystals corroded by calcite in a fragment of the clotted-peloidal boundstone surrounded by blocky calcite

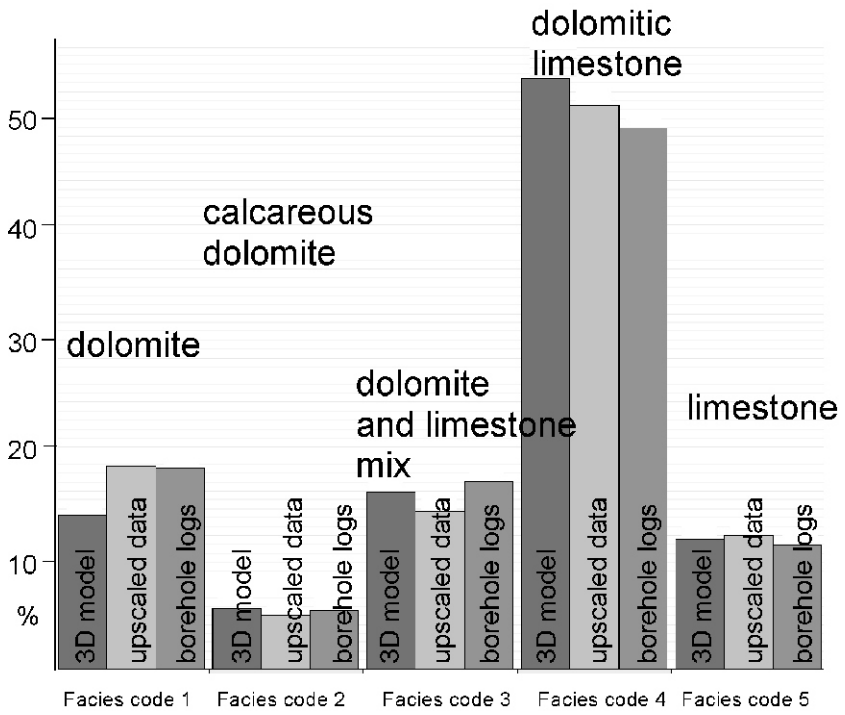

Fig. 6. Quality assurance of the reef model by comparison of the input data from the boreholes, with the upscaled data (data ascribed to the 3D grid) and the volumetric data of the (uneroded) 3D model

Dolomite (facies codes 1–3) is slightly underrepresented in the 3D model

A curved covariance of ^{13}C and ^{18}O can be observed in the data from hand specimens (Fig. 8D). The curves are characterized by a rapidly decreasing ^{18}O coupled with a gradual decrease of ^{13}C. The curves show similar shapes but, depending on the samples, have different ^{13}C and ^{18}O ranges, similar to but shallower than those suggested for the Capitan reef limestone (Bishop et al., 2014). The interpolation of the stable isotope point data from the entire Buchenberg reef shows a patchy, irregular pattern without trends (Fig. 13).

Sr ISOTOPES

The $^{87}Sr/^{86}Sr$ of the reef carbonates (Fig. 14A) ranges from 0.7075 to 0.7088. Three samples from basinal dolomite show higher values ranging from 0.70886 to 0.70911. In the Buchenberg section (Fig. 3) the $^{87}Sr/^{86}Sr$ ratios decrease from a maximum in the basal dolomite to a minimum within the reef carbonate followed by an increase at the reef top. As a whole, reef dolomite and limestone $^{87}Sr/^{86}Sr$ have similar ranges. Strontium concentrations measured from the 3 hand specimens range from ~30 to 130 ppm and show a curved covariance with the Ca/Mg ratio (Fig. 14B).

DISCUSSION

INCONSISTENCIES WITH CURRENT DOLOMITIZATION MODELS

Three lines of evidence indicate that the dolomite studied is not compatible with current dolomitization models: the paragenesis, the geometry of the dolomite bodies, and the stable isotope geochemistry.

Reef paragenesis. The macroscopic and microscopic features of the reefs studied are compatible with a marine paragenesis. The clotted-peloidal fabric indicates that the matrix is probably microbial in origin (Paul, 1980, 1995) and preserves very high residual primary porosity. The isopachous cement rims lining the pore spaces and the absence of pendant or meniscus cements indicate a marine-phreatic diagenetic environment. The large pore spaces could, in principle, result from the total removal of evaporites by leaching, but the absence of corrosion features in fossils and cements make this option unlikely, an assumption also supported by the lack of detectable amounts of evaporite minerals in XRD, with the few exceptions from the Römerstein reef. The local presence of blocky calcite and dolomite is not indicative of a particular diagenetic environment (Flügel, 2000). The reefs record, therefore, a simple paragenesis of marine origin. A peculiarity of the dolomite studied is the observation that the dolomite cannot be a “replacement” dolomite in the sense of Purser et al. (1994). The proper meaning of “replacement” is that dolomite replaces a pre-existing calcite fabric and is, therefore, the younger phase. The partly dolomitic lithologies of the reefs studied show the opposite, namely dolomite corroded by, therefore older than, calcite. The calcite crystals are certainly not a dedolomite, which is normally seen as dolomite rhombs replaced by calcite associated with a complete destruction of the depositional fabric (e.g., Schönherr et al., 2018). This is the first incompatibility of the rocks studied with current dolomitization models.

Dolomite geometries. The second incompatibility with current dolomitization models comprises the dolomite geometries. It is clear that the 3D model is only a very coarse approximation of the true parameter distribution in the reef. The randomly taken hand specimens suggest property changes

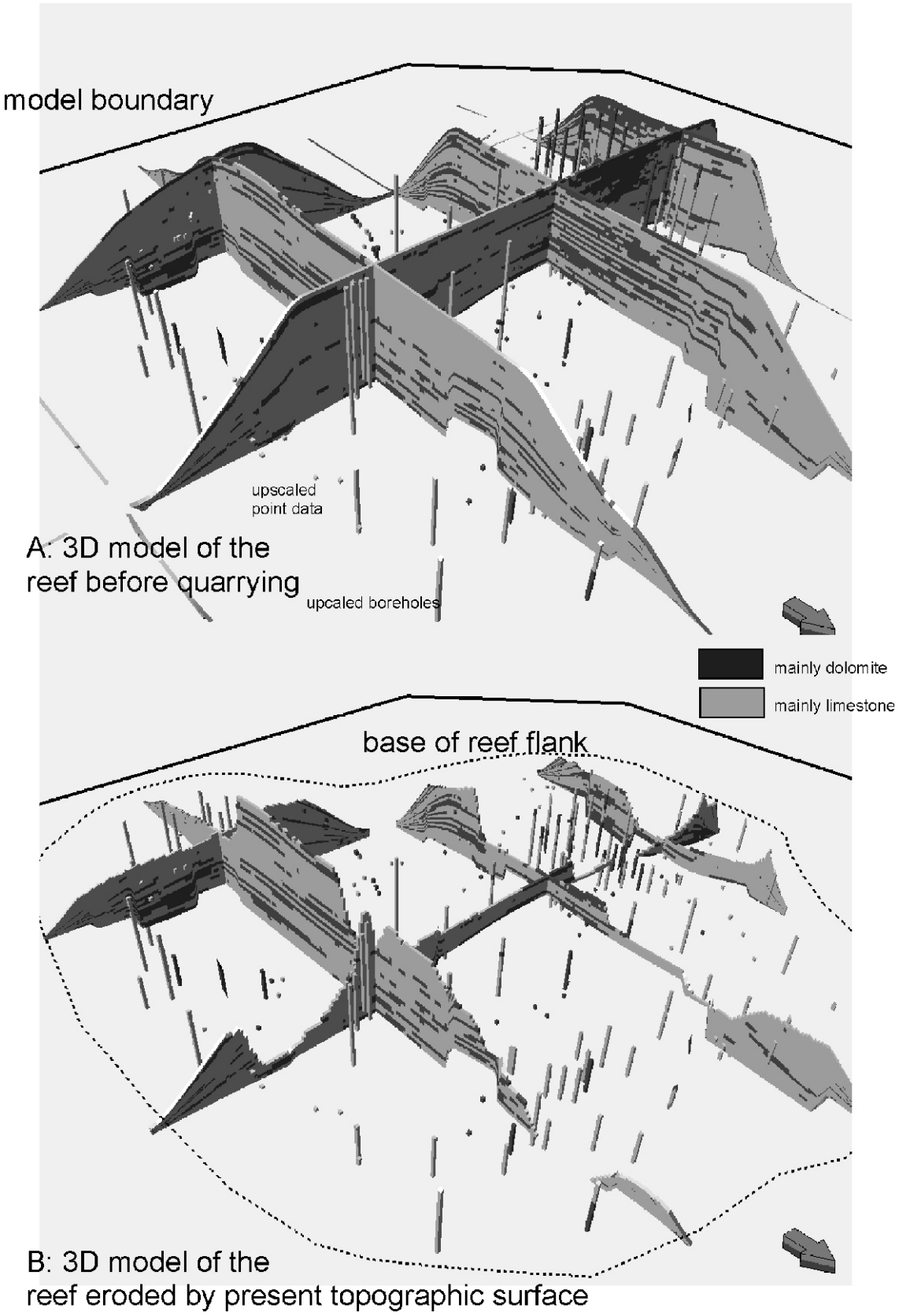

Fig. 7. Oblique aerial view from the NE of a fence of the 3D model showing the distribution of dolomite and limestone in the Buchenberg reef

All dolomite forms laterally discontinuous bodies; a larger dolomite body was present in the SW part of the reef (A) but is now completely quarried (B); B shows the 3D model with all cells above the present topography removed; the fences are 2 vertically exaggerated

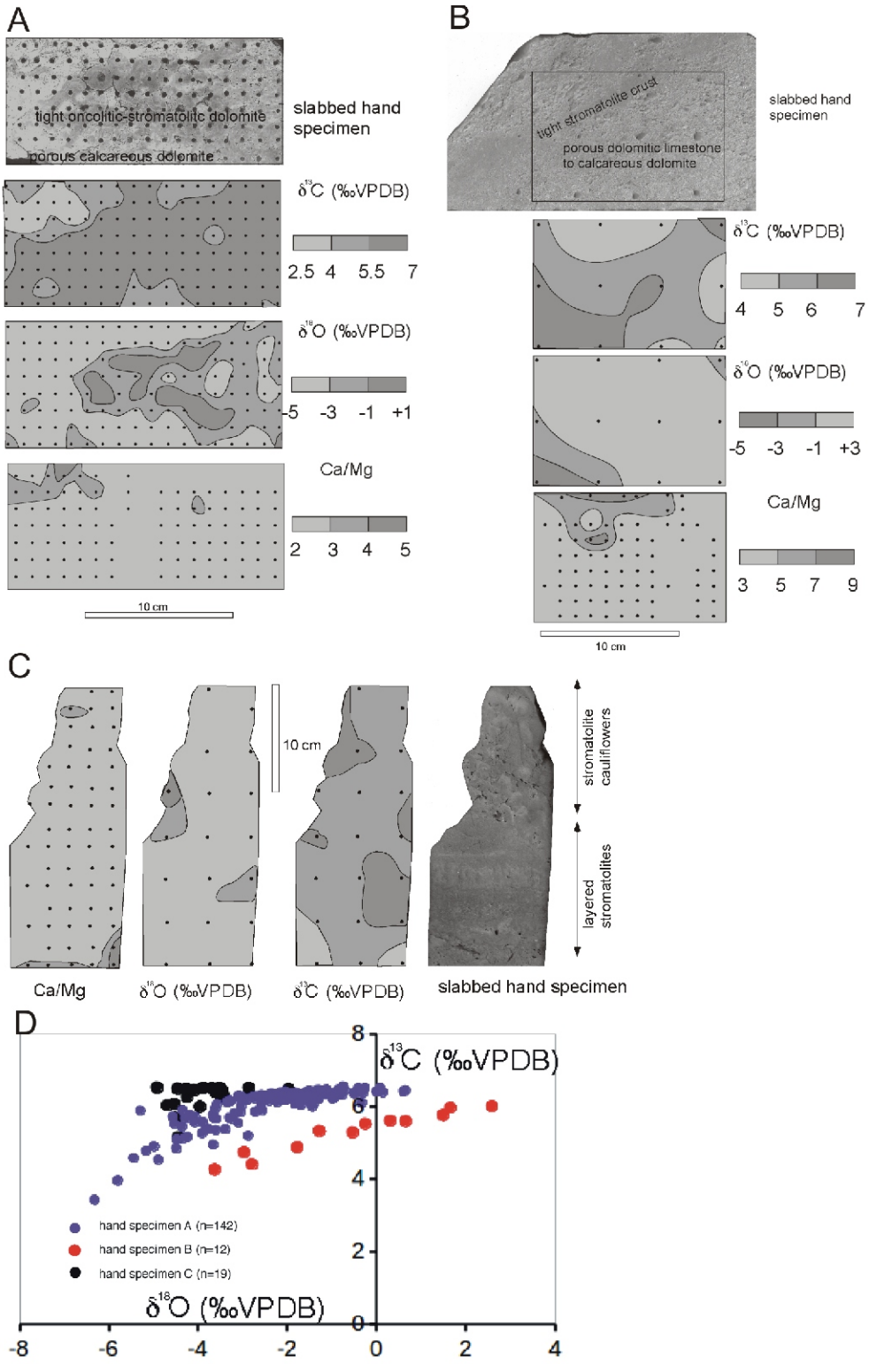

Fig. 8. Interpolated 2D distribution of properties of the hand specimens

Black dots are sample locations. All interpolations indicate a gradual change of the parameters measured. **A** – an oncolitic dolomite with a tight, darker coloured, part in the centre of the sample; **B** – a massive, structureless, calcareous dolomite from the reef interior with a tight interval, inclined to the left, in the central part of the sample; **C** – a stromatolitic, dolomitic boundstone with cm-size stromatolite cauliflowers (with tight, darker coloured layers and bright, porous layers) in the upper part and more layered stromatolites in the lower part. In none of the samples does a clear relationship exist between the measured parameters and the rock fabric or porosity except for (A), where the tight part roughly overlaps the more dolomitic area and the heaviest oxygen isotope values; **D** – the cross-plot of the carbon and oxygen isotopes of the hand specimens showing the curved co-variance of oxygen and carbon in samples A and B

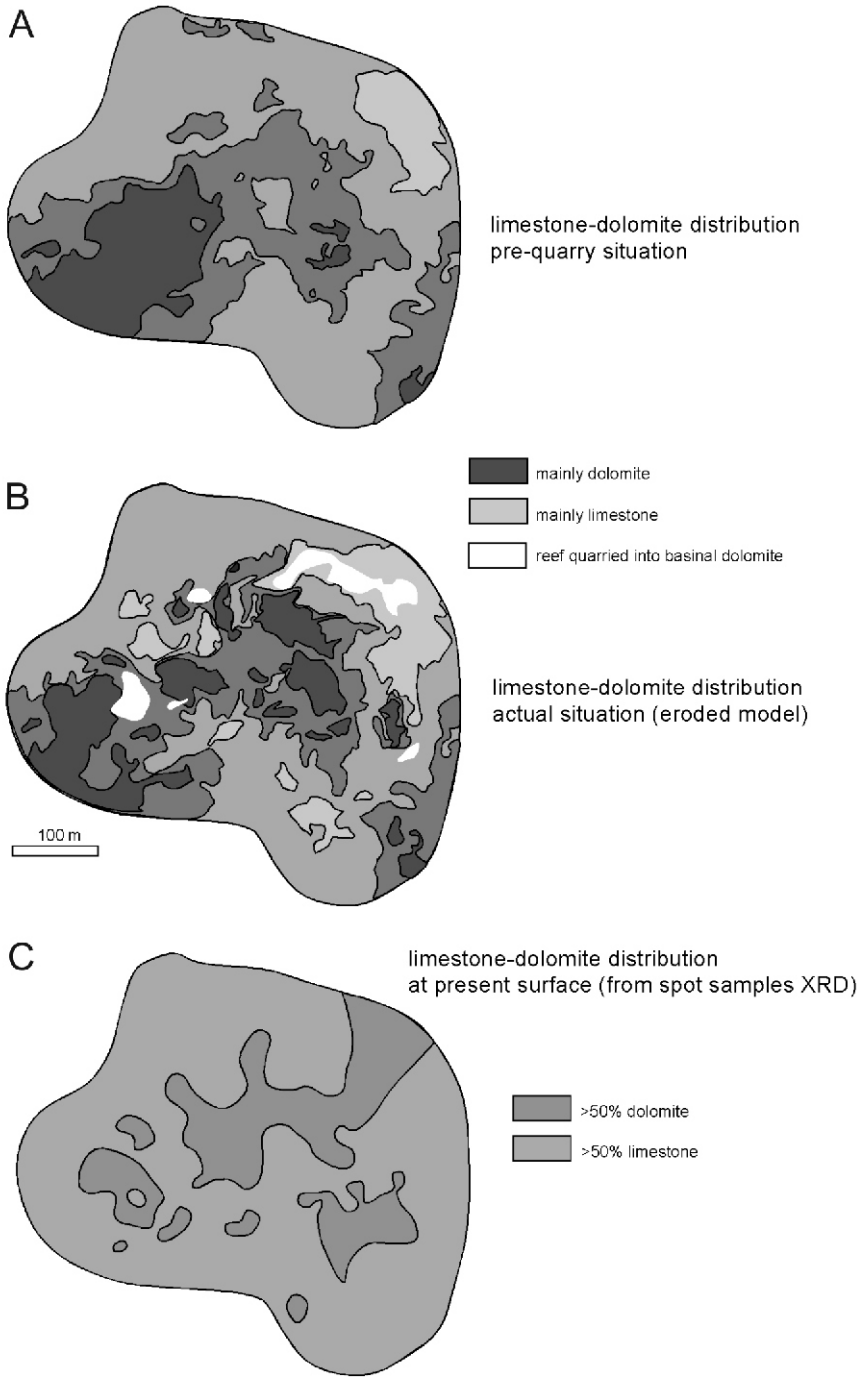

Fig. 9. Average maps of the lithology from the 3D model of the Buchenberg reef

The map of the complete reef (A) shows a slight dominance of dolomite in the SW part of the reef (see also Fig. 7A), which is very similar in the model limited upwards by the present topographic surface (B). The interpolation of the XRD point data alone (C) show slightly more limestone in the flanks as compared to the map of A and B. The distribution of limestone and dolomite does not follow any regular pattern

at the decimetre scale (Fig. 8), a detail which cannot be modeled for a comparatively large reef. The distribution of limestone and dolomite, as quantified in the present model, is in fact a model of the lithology prevailing in certain parts, but, as the XRD and borehole data indicate, pure limestone and pure dolomite (0% of the other mineralogy) are comparatively rare (Fig. 11C). Various hydrological models for fluid flow have been developed, all of which were expected to show distinct dolomite-limestone boundaries or dolomitization front geometries. The expected dolomite geometries and the expected isotopic signature have been compiled in Figure 15 using the models in Wilson et al. (1990) and Vahrenkamp and Swart (1994). A hydrothermal dolomitization should result in dolomite bodies preferably along faults and fractures, ideally with a “Christmas tree” (lateral fingering from a vertical stem) geometry, but this is not observed. A mixing zone could develop

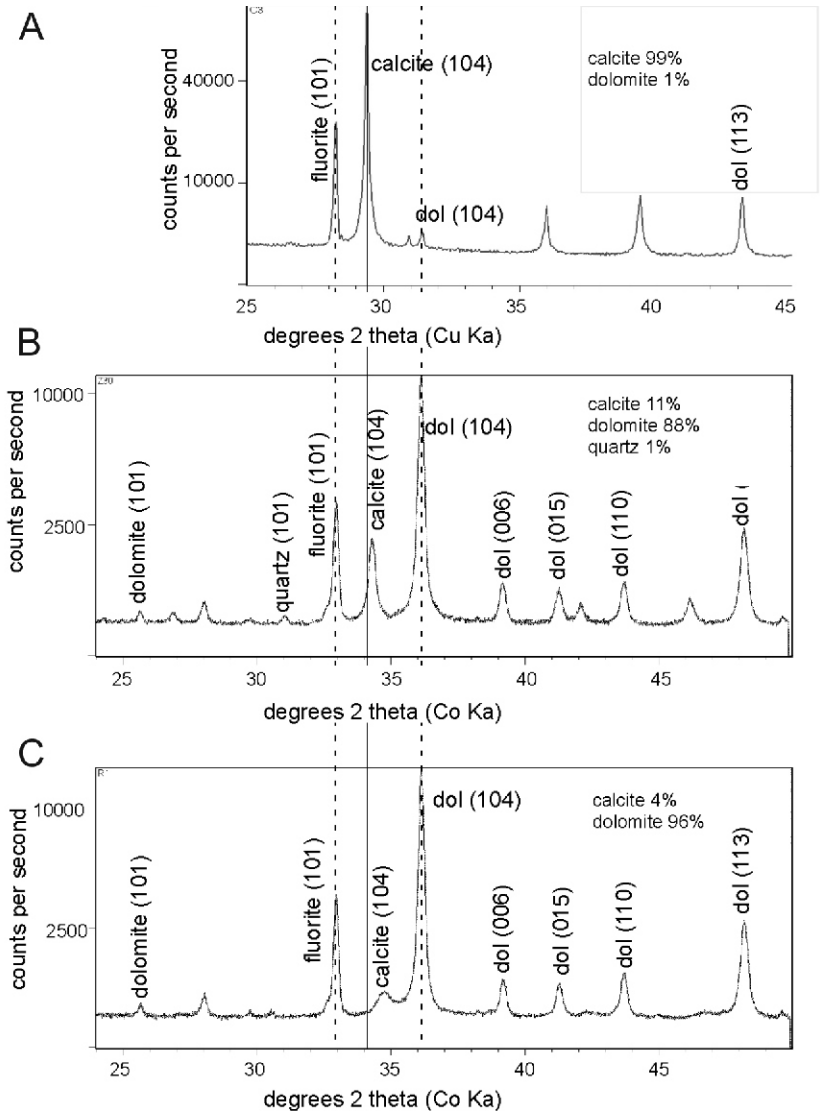

Fig. 10. X-ray diffractograms of the reef carbonates

A – an almost pure calcite from the Totenstein reef, calcite ordering peaks are well developed; **B** – a dolomite containing calcite from the Buchenberg; **C** – a dolomite from the Römerstein reef containing small amounts of calcite with a distinct peak shift and poorly developed ordering reflections. Dolomite (104) reflection in all cases shows no peak shift, indicating nearly stoichiometric dolomite. Calcite peak shift (with respect to the thin vertical line indicating a Mg-free calcite) corresponds to ~4 mol% $MgCO_3$ in (C), the shift in (B) to ~2 mol% $MgCO_3$. The fluorite peak is from the internal standard

as result of a meteoric water lens mixing with seawater during intermittent reef emersion (see also Swart, 2015). This should be associated with a saucer-shaped dolomite body, but this dolomite geometry is not observed either. A normal marine dolomitization model (seawater pumped laterally through the flanks) should result in preferentially dolomitic flanks, but the opposite is observed. Dolomitizing fluids derived from shale compaction should also result in preferentially dolomitic reef flanks. The laterally discontinuous dolomite intervals of the Buchenberg are, therefore, difficult to explain with current dolomitization models. This includes the brine sinking model, which is the standard model for Zechstein dolomite so far (e.g., Clark, 1980). In this case, dolomite geometries should show a downward increase in limestone in a partially dolomitic reef, geometrically similar to a mixing zone dolomite (but with different geochemical signal, see Fig. 15). The rareness absence of evaporites in the XRD traces is another, non-geometrical, argument against such evaporitic brines. It is, therefore, difficult to reconcile the geometries of the dolomite bodies in the Buchenberg with any of the existing fluid flow models.

It could be argued that, because of similarities with the hydrothermal model, the dolomite bodies of the Buchenberg are in fact remnants of a hydrothermal dolomite body, where the fracture(s) related to these bodies remained unrecognized. The main geometrical argument against a hydrothermal dolomitization is the lack of a “stem” or any linear element rooted in the bottom part of the reef, and the hydrothermal dolomite model is a very unlikely scenario.

Geochemical data. The third inconsistency with current dolomitization models is the ^{13}C values, which are different in limestone and dolomite in the same stratigraphic succession, of

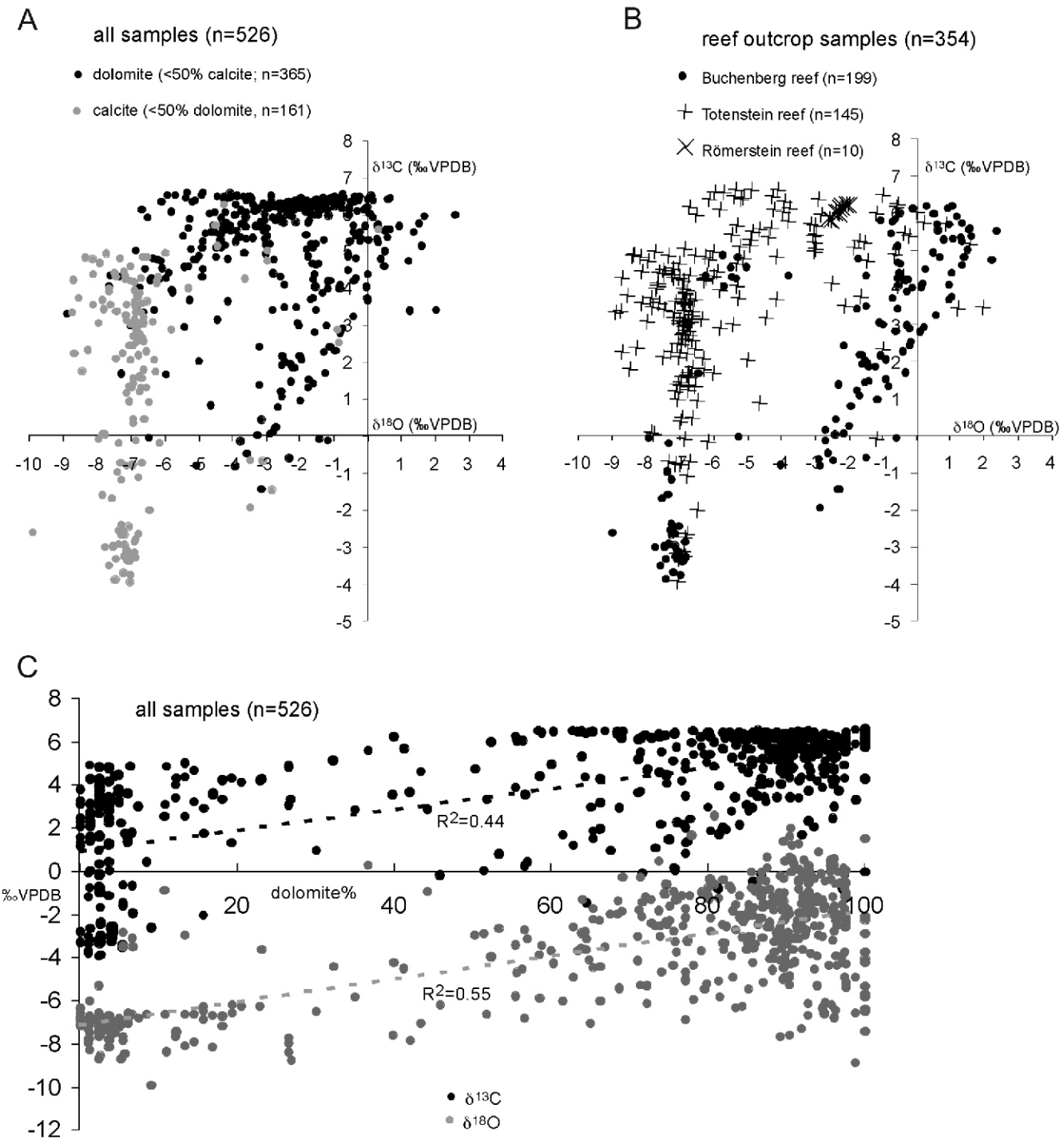

Fig. 11. Cross-plots of stable isotope values for limestone and dolomite (A), sample provenance (B), and stable isotopes *versus* dolomite percentage (C)

(A) and (B) cover a field predicted for fluid-rock interaction of a marine carbonate with isotopically lighter fluids, (C) shows moderate correlation (stippled lines) of stable isotopes and dolomite content; all diagrams show clearly that the maximum values of limestone and dolomite ^{13}C differ by ~1.5‰

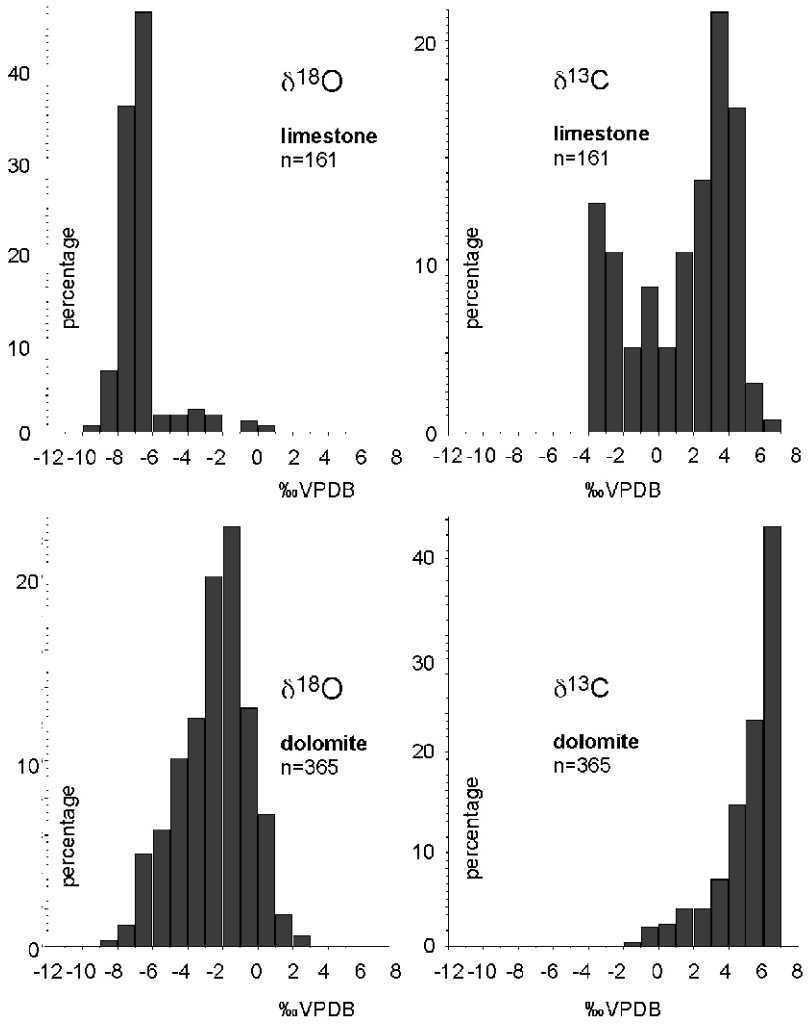

Fig. 12. The histograms for ^{13}C and ^{18}O show the differences between dolomite and limestone, particularly the bimodal limestone ^{13}C and the shift of limestone ^{18}O relative to the dolomite values

the reefs. This is not foreseen in any dolomitization model: because of the low water-rock ratios invoked in all these flow models, ^{13}C is thought to remain unmodified with respect to the precursor calcite (e.g., Carmichael et al., 2008; Swart, 2015). This means that dolomite produced by a dolomitization process involving fluid flow, and the calcite precursor, should show the same ^{13}C. This is not the case in the reef carbonates studied.

It could be argued that heavier dolomite ^{13}C was caused by oxidation of organic matter before the transformation into dolomite. It is unlikely, however, that this process operated preferentially in a calcite precursor of the dolomite studied, because dolomite and limestone show the same fabric, and, therefore, the amount of original organic matter was probably similar.

EQUIVOCAL ISOTOPE PATTERN

Strontium isotopes. The $^{87}Sr/^{86}Sr$ values measured are more radiogenic than those of assumed Late Permian seawater (~0.7068; Korte and Ullmann, 2016), but similar to those reported from Zechstein reefs in Poland (Peryt et al., 2016). The $^{87}Sr/^{86}Sr$ signal of both dolomite *and* limestone are similar. Because this includes the basinal dolomite, the reefs or reef dolomite cannot be considered a radiogenic anomaly, unlike many dolomite bodies elsewhere. It is possible that the marginal, land-locked areas of the essentially isolated Permian sea had higher $^{87}Sr/^{86}Sr$ than open ocean or evaporitic settings, particularly directly after the Upper Permian transgression onto the eroded Variscan basement. But the marine fauna of the basinal rocks directly above the unconformity indicates near-normal marine conditions. The radiogenic deviation of these $^{87}Sr/^{86}Sr$ ratios from inferred Late Permian seawater is significantly higher than in the equally semi-enclosed Middle Triassic Germanic Basin (cf. Korte et al., 2003), calling for a different cause of the radiogenic Sr signature.

The depositional concentration of Sr in carbonates ranges from hundreds to thousands of ppm (e.g., Bathurst, 1971). During diagenetic loss of Sr, the $^{87}Sr/^{86}Sr$ ratio in many cases increases (e.g., Veizer, 1983). This is usually understood as reflecting the changing isotopic composition of the pore fluid and, therefore, fluid flow through the rock during recrystallization. A causal relationship with freshwater is unproven, though. A much simpler alternative is that the diagenetic Sr loss, in a semi-closed diagenetic system, is associated with a preferential loss of the light Sr isotope and not necessarily with radiogenic fluids percolating through the rock during diagenesis. The ra-

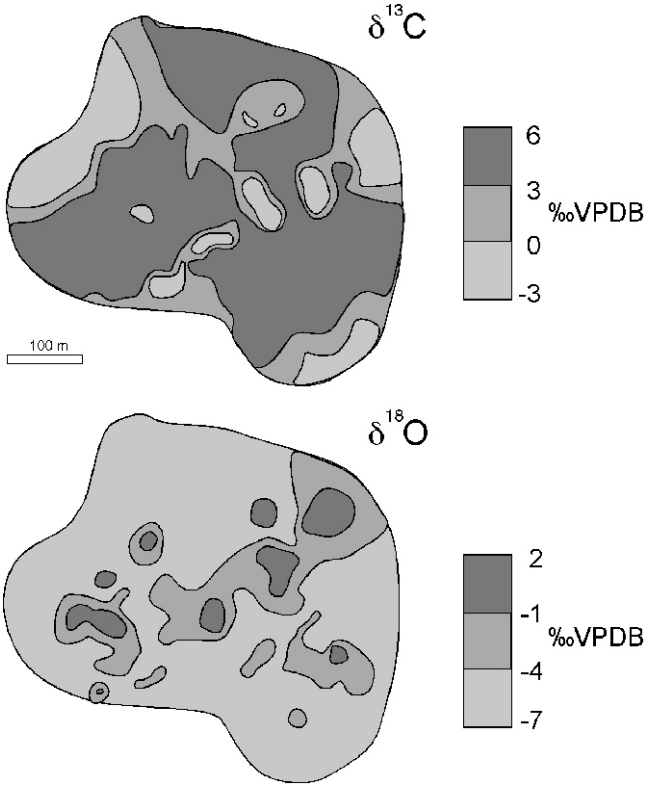

Fig. 13. Isotope maps of the *Buchenberg* reef obtained from a 2D interpolation of the point data

Both ^{13}C and ^{18}O show a patchy pattern without linear or reef geometry-related trends; for the legend see Figure 4

diogenic $^{87}Sr/^{86}Sr$ is not considered here as proof that the originally marine pore fluids were displaced during diagenesis.

Stable isotopes. Part of the observed stable isotope data spread is certainly due to a sampling effect. The isotope samples are significantly smaller in quantity than material required for XRD analysis. This means that that a mix of pure calcite and pure dolomite crystals was drilled for isotope study in many cases. Because of this, average isotope values probably occur in many samples.

In spite of the above uncertainty, a pattern emerges which clearly shows that more negative values prevail in calcite, whereas dolomite shows less variability than limestone (Fig. 12). The negative limestone ^{13}C values are incompatible with a Permian seawater signature (cf. Bishop et al., 2014), one of the highest ^{13}C of the Phanerozoic. Using fluid flow models, the negative ^{13}C values require diagenetic modification of a marine isotope signal by different fluids. In fact, current models for isotope resetting (Banner and Hanson, 1990) suggest that the marine pore fluids in this case were displaced by isotopically light fluids, modifying the rock isotope signal by increasing the water-rock ratios. The clear negative trend of carbon isotope values in calcite (Fig. 11) is similar to the "inverted J" curve of Lohmann (1987), which is thought to be typical of freshwater diagenesis. Such freshwater could be a meteoric lens developed during reef exposure, or artesian freshwater entering the reef from below. In either case, the stable isotope values should decrease towards the source of freshwater, but a vertical isotope trend is not observed in the reefs studied (Fig. 3). Meteoric waters of artesian origin would enter the reefs *via* fractures in the basement, but the isotope pattern is patchy and shows no linear trends (Fig. 13).

It might be argued that the negative calcite stable isotope values document freshwater diagenesis *before* dolomitzation occurred. Such a diagenetic path has been suggested by Clark

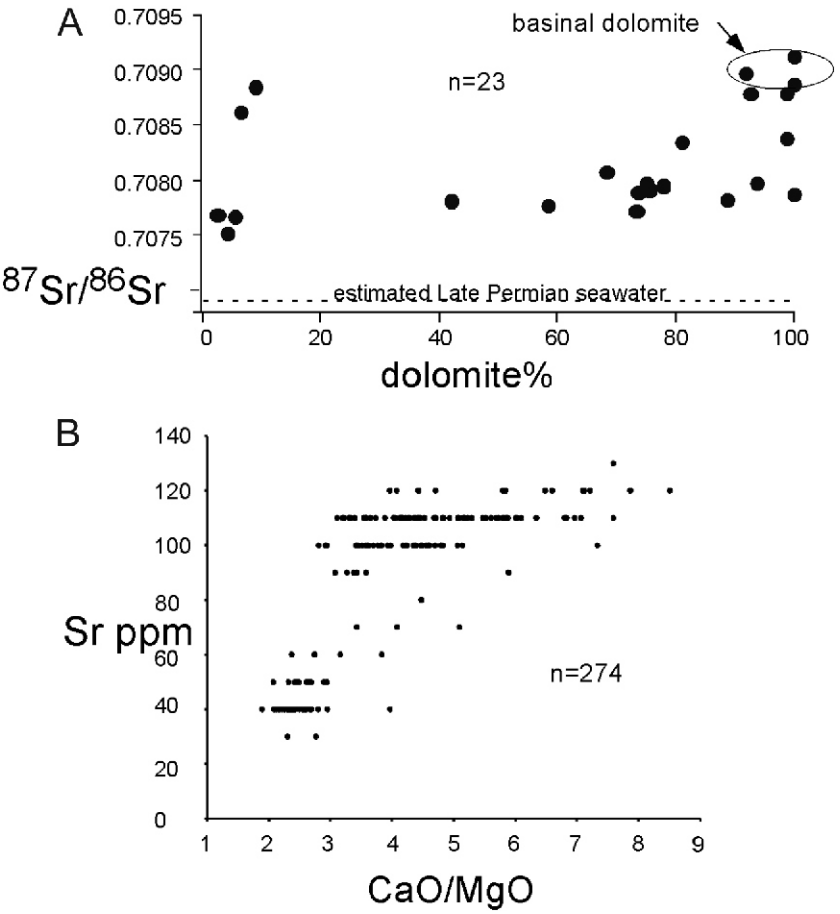

Fig. 14A – $^{87}Sr/^{86}Sr$ ratios of the reef and basinal carbonates *versus* the dolomite content, all data are more radiogenic than inferred open marine Late Permian seawater, which corresponds to ~0.7069, the range of values is similar for limestone and dolomite suggesting similar pore fluids accounting for diagenesis; B – the relationships between Sr concentration, measured in increments of 10 ppm, and the CaO/MgO ratio, measured with XRF, the data show that Sr concentrations decrease with decreasing CaO/MgO ratio

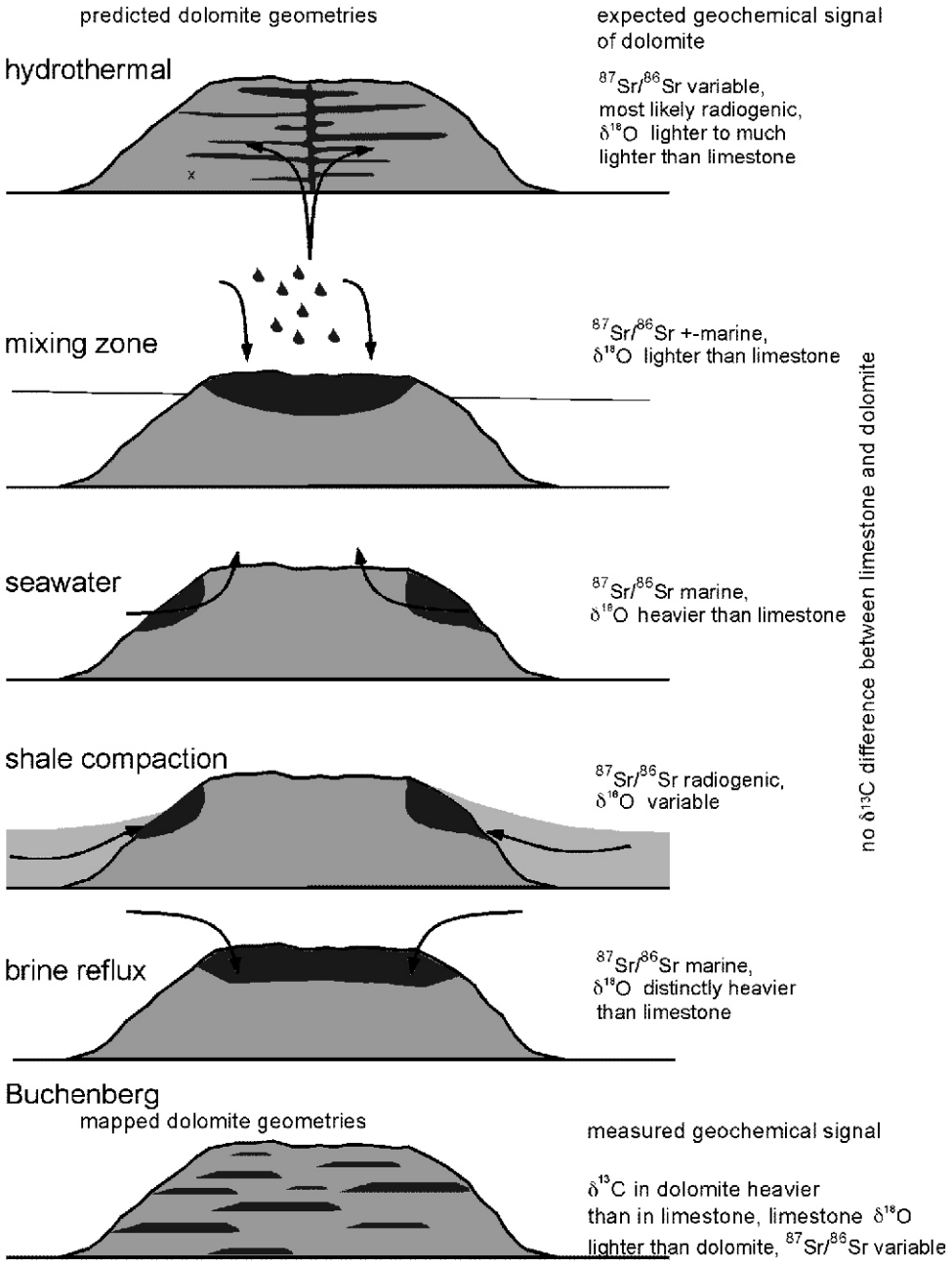

Fig. 15. Sketch of dolomite geometries expected from various fluid flow models for an isolated carbonate such as the reefs studied and the likely isotopic signal of dolomite

Compiled from data in Wilson et al. (1990) and Swart (2015); arrows indicate flow direction of dolomitizing fluids; the dolomite geometries (dark grey) mapped from the Buchenberg reef are difficult to reconcile with any geometrical predictions

(1980; first freshwater diagenesis and then dolomitization). If such diagenetically modified limestone would be the precursor of a dolomite created by fluid flow, limestone ^{13}C should be preserved in dolomite, and dolomite should show a negative maximum, too. Alternatively, if very high water-rock ratios (and a substantial assumption of current dolomitization models thus being violated) are assumed, this would invariably have reset all oxygen isotopes to the ^{18}O values of the fluid. The expected narrow range of ^{18}O values is not observed, and such a diagenetic pathway seems unlikely.

The stable isotope pattern is, therefore, not easily reconciled with a freshwater diagenetic model, and the observed pattern can also be explained by different processes. One is vital fractionation, because the reefs studied consist of biominerals (reflected in the various stromatolite forms and the oncolites dominating the reefs), and disequilibrium effects caused by high rates of precipitation. Disequilibrium fractionation in biogenic carbonates is relatively well known in modern environments (McConnaughey, 1989; Bajnai et al., 2018) and appears to the rule rather than the exception (Daëron et al., 2019), but is poorly known in ancient carbonates, where it is considered to be erased by the so-called diagenetic filter (Gischler et al., 2009). Isotope resetting by isotopically light fluids and disequilibrium fractionation can show the same effect on stable isotopes, namely the co-variance of ^{13}C and ^{18}O (data compiled in Swart, 2015).

Fast precipitation rates of calcite can also lead to depletions in both ^{13}C and ^{18}O, with a pattern similar to that reported herein (cf. McConnaughey, 2003). The reefs grew at faster rates than the equivalent basinal succession. If fractionation due to growth rate played a role, then the slower growing reef flanks should show heavier values than the reef interior, but this cannot be quantified and tested at the moment because of the comparatively low number of samples from this part of the reefs.

Another, purely diagenetic, option seems equally likely at this moment. It is clear that the reefs now consist of Mg-free calcite and near-stoichiometric dolomite. It is very unlikely, though, that all the reef calcite present formed as a primarily Mg-free polymorph such as aragonite and LMC, but originally had a wide range of Mg concentrations similar to what is observed in the modern environment (cf. Bathurst, 1971). The negative to very negative calcite values could simply be the result of preferential loss of the heavier stable isotopes associated with Mg loss during diagenesis: the higher the original amount of Mg in the calcite, the stronger the negative diagenetic shift. In this case, the most negative calcites originally had the highest Mg content. These could not recrystallize to dolomite when they had less than the critical amount of $MgCO_3$ necessary for such recrystallization. Empirical data indicate that dolomite has a lower limit of ~40 mol% $MgCO_3$ (e.g., Searl, 1994). The most positive stable isotope values of the calcite studied would record primarily Mg-free polymorphs, either LMC or aragonite. The poorly developed negative trend of dolomite isotopes could be an effect of the reduced Mg loss as compared to most calcites.

The proposed effect could be quantified from modern HMC, for instance from echinoderms, but appears uncertain at this moment because only few data exist (Kroh and Nebelsick, 2010), Weber and Raup (1968) found no evidence for a correlation with Mg-loss, albeit on a very limited comparative database. The degree of diagenetic alteration of ^{13}C and ^{18}O values in HMC cannot be predicted at present without reliable comparative data from modern settings.

ALTERNATIVE DOLOMITE GENESIS

The paragenetic, geometrical and geochemical data presented in this study suggest that the dolomite studied is not easily explained in terms of current dolomitization models, and requires an alternative explanation. A transformation of calcite to dolomite is considered possible without fluid flow, in a completely stationary pore fluid regime, if a VHMC with a chemical composition similar to that of dolomite was the precursor.

Very high Mg calcite is invariably the precursor phase of dolomite in high temperature experiments, and dolomite practically always originates from recrystallization of a VHMC (Gregg et al., 2015; Kaczmarek et al., 2017). In contrast to dolomite, a VHMC with >50% $MgCO_3$ can be synthesized in the laboratory under ambient conditions (Zhang et al., 2010, 2012a, b), with some experiments involving microbe cultures (Vasconcelos et al., 1995). According to Gregg et al. (2015) "...this transition from … VHMC to ordered dolomite remains to be demonstrated experimentally at low temperature.". This experiment has not failed but has never been attempted. Recrystallization of a VHMC to dolomite is an isochemical conversion, where only the crystal system and density change, and it is not necessary to add material to the precursor phase. The stable isotope signal would be inherited from the VHMC precursor and, therefore, show heavier ^{13}C than equivalent LMC. It is probably no coincidence that the heaviest ^{13}C values of limestone and dolomite differ by ~1.5‰. A carbonate, dolomite or VHMC, containing 50 mol% $MgCO_3$, is ~1–2‰ heavier than equivalent Mg-free LMC (Jimenez-Lopez et al., 2006; Horita, 2013). A VHMC could form naturally in the reefs studied, either mediated or induced by microbes, or independently of vital effects, and simply recrystallized to dolomite, without fluid flow, in a semi-closed diagenetic system. In spite of potential recrystallization (Kaczmarek and Sibley, 2014), the dolomite stabilized earlier than the calcite (Fig. 5D), and this also explains the lower degree of variability in stable isotope composition (Fig. 12). VHMC containing >50 mol% $MgCO_3$ recrystallized to dolomite, whereas HMC with <~50 mol% $MgCO_3$ lost its entire Mg during many recrystallization events until the present Mg-free, stable LMC was formed. The stabilization of both minerals was accompanied by a gradual loss of the heavier stable isotopes following a curved co-variance (Fig. 8D) with the overall shape of an "inverted J" curve (Fig. 11A, B). Only very few relics of Mg-containing calcite are preserved (Fig. 10), and one of the open questions is how the original Mg content of ancient calcite can be quantified. The loss of Sr also affected both minerals, and the increase of the $^{87}Sr/^{86}Sr$ ratio was most likely only related to the preferential diagenetic loss of ^{86}Sr in a semi-closed system.

CONCLUSIONS

Three-dimensional modeling of partially dolomitic carbonates is a step necessary to quantify dolomite geometries and to test these against dolomitization models. In the Zechstein reef modelled, the dolomite geometries are all isolated and are incompatible with all dolomitization models at hand.

Comparative analysis of stable isotopes of limestone and dolomite can help to test whether dolomite can be a recrystallized VHMC. When the maximum values of ^{13}C of calcite and dolomite differ by 1–2‰, a recrystallized depositional VHMC with a chemical composition similar to that of dolomite is likely.

The stable isotope pattern of the Zechstein reefs conforms to one produced by increasing water-rock interactions of a marine carbonate with isotopically lighter, radiogenic fluids. In view of the lack of evidence for fluid flow, it is more likely that the isotope pattern documents the result of vital effects, the effect of high precipitation rates, or preferential loss of heavy stable isotopes associated with Mg loss during diagenesis, in a semi-closed diagenetic environment. The radiogenic $^{87}Sr/^{86}Sr$ of the carbonates studied can be explained as preferential loss of ^{86}Sr in parallel with diagenetic reduction of the Sr concentration.

Acknowledgements. Schlumberger is thanked for providing free research licenses for their modelling program *Petrel*. The Geological Service of Thuringia (Erfurt) provided copies of the Buchenberg borehole files. The Landratsamt Saale-Orla Kreis (Schleiz) granted permission to sample in the nature reserve of the Thuringian reefs. The stable isotope analyses were carried out by A. Pack (Göttingen) and M. Joachimski (Erlangen). Strontium isotopes were analysed by N. Nolte-Moser (Göttingen). Thin sections were manufactured by M. Josuweit, U. Hemmerling (Clausthal) and Precilab (Carrolton, Texas). X-ray diffraction analyses were carried out by W. Ehrmann (Leipzig) and staff of the institute for Radioactive Waste Research (Clausthal), and XRF analyses by F. Türck (Clausthal). The journal reviewers M. Jasionowski and A. Poszytek provided constructive suggestions for improvement. The support of all institutions and individuals is gratefully acknowledged.

REFERENCES

Bajnai, D., Fiebig, J., Tomašových, A., Milner Garcia, S., Rollion-Bard, C., Raddatz, J. Löffler, N., Primo-Ramos, C., Brand, U., 2018. Assessing kinetic fractionation in brachiopod calcite using clumped isotopes. Springer Scientific Reports, **8**, article number, 533.

Banner, J. Hanson, G., 1990. Calculations of simultaneous isotopic and trace element variations during water-rock interaction with applications to carbonate diagenesis. Geochimica et Cosmochimica Acta, **54**: 3123–3137.

Bathurst, R.G.C., 1971. Carbonate Sediments and Their Diagenesis. Elsevier, Amsterdam.

Bishop, J.W., Osleger, D.A., Montañez, I.P., Sumner, D.Y., 2014. Meteoric diagenesis and fluid-rock interaction in the Middle Permian Capitan backreef: Yates Formation, Slaughter Canyon, New Mexico. AAPG Bulletin, **98**: 1495–1519.

Carmichael, S.K., Ferry, J.M., McDonough, W.F., 2008. Formation of replacement dolomite in the Latemar carbonate buildup, dolomites, northern Italy: part 1. Field relations, mineralogy, and geochemistry. American Journal of Science, **308**: 851–884.

Clark, D.N.,1980. The diagenesis of Zechstein carbonate sediments. Contributions to Sedimentology, **9**: 167–203.

Daëron, M., Drysdale, R,N., Peral, M., Huyghe, D., Blamart, D., Coplen, T.B., Lartaud, F., Zanchetta, G., 2019. Most Earth-surface calcites precipitate out of isotopic equilibrium. Nature Communications, **10**: 429.

Flügel, E., 2000. Microfacies Analysis of Limestones. Springer, Berlin.

Gabellone, T., Whitaker, F., 2016. Secular variations in seawater chemistry controlling dolomitization in shallow reflux systems: insights from reactive transport modelling. Sedimentology, **63**: 1233–1259.

Gischler, E., Swart, P.k., Lomando, A.J., 2009. Stable isotopes of carbon and oxygen in modern sediments of carbonate platforms, barrier reefs, atolls and ramps: patterns and implications. IAS Special Publications, **41**: 61–74.

Gregg, J.M., Bish, D.L., Kaczmarek, S., Machel, H.G., 2015. Mineralogy, nucleation and growth of dolomite in the laboratory and sedimentary environment: a review. Sedimentology, **62**: 1749–1769.

Horita, J., 2013. Oxygen and carbon isotope fractionation in the system dolomite–water–CO_2 to elevated temperatures. Geochimica et Cosmochimica Acta, **129**: 111–124.

Jasionowski, M., Peryt, T.M., Durakiewicz, T., 2014. Polyphase dolomitisation of the Wuchiapingian Zechstein Limestone (Ca1) isolated reefs (Wolsztyn Palaeo-Ridge, Fore-Sudetic Monocline, SW Poland). Geological Quarterly, **58** (3): 503–520.

Jimenez-Lopez, C., Romaek, C.S., Caballero, E., 2006. Carbon isotope fractionation in synthetic magnesian calcite. Geochimica et Cosmochimica Acta, **70**: 1163–1171.

Kaczmarek, S.E, Sibley, D.F., 2014. Direct physical evidence of dolomite recrystallization. Sedimentology, **61**: 1862–1882.

Kaczmarek, S.E., Gregg, J.M., Bish, D.L., Machel, H.G., Fouke, B.W., 2017. Dolomite, very high-magnesium calcite, and microbes – implications for the microbial model of dolomitization. SEPM Special Publications, **109**: 7–20.

Kerkmann, K., 1969. Riffe und Algenbänke im Zechstein von Thüringen. Freiberger Forschungshefte, **C252**: 1–85.

Kim, S.T., Mucci, A., Taylor, B.E., 2007. Phosphoric acid fractionation factors for calcite and aragonite between 25 and 75°C: revisited. Chemical Geology, **246**: 135–146.

Korte, C., Ullmann, C.V., 2016. Permian strontium isotope stratigraphy. Geological Society Special Publications, **450**: 105–118.

Korte, C., Kozur, H., Bruckschen, P., Veizer, J., 2003. Strontium isotope evolution of of Late Permian and Triassic seawater. Geochmica et Cosmochimica Acta, **67**: 47–62.

Kroh, A,, Nebelsick J.H., 2010. Echinoderms and Oligo-Miocene carbonate systems: potential applications in sedimentology and environmental reconstruction. IAS Special Publications, **42**: 201–228.

Lohmann, K.C., 1987. Geochemical patterns of meteoric diagenetic systems and their application to the study of paleokarst. In: Paleokarst (eds. N.P. James and P.W. Choquette): 58–80. Springer, Berlin.

Machel, H.G., 2004. Concepts and models of dolomitization: a critical reappraisal. Geological Society Special Publications, **235**: 7–63.

McConnaughey, T., 1989. ^{13}C and ^{18}O isotopic disequilibrium in biological carbonates: I. Patterns. Geochimica et Cosmochimica Acta, **53**: 151–162.

McConnaughey, T.A., 2003. Sub-equilibrium ^{18}O and ^{13}C levels in biological carbonates: carbonate and kinetic models. Coral Reefs, **22**: 316–327.

Paul, J., 1980. Upper Permian algal stromatolitic reefs, Harz Mountains (F.R. Germany). Contributions to Sedimentology, **9**: 253–268.

Paul, J., 1995. Stromatolite reefs of the Upper Permian Zechstein Basin (Central Europe). Facies, **32**: 28–31.

Peryt, T.M., Raczyński, P., Peryt, D., Chłódek, K., Mikołajewski, Z., 2016. Sedimentary history and biota of the Zechstein Limestone (Permian, Wuchiapingian) of the Jabłonna reef in western Poland. Annales Societatis Geologorum Poloniae, **86**: 379–413.

Purser, B.H., Tucker, M.E., Zenger, D.H., 1994. Problems, progress and future research concerning dolomites and dolomitization. IAS Special Publications, **21**: 3–20.

Reijers, T.J.A., 2012. Sedimentology and diagenesis as 'hydrocarbon exploration tools' in the Late Permian Zechstein-2 Carbonate Member (NE Netherlands). Geologos, **18**: 163–195.

Rosenbaum, J., Sheppard, S.M., 1986. An isotopic study of siderites, dolomites and ankerites at high temperatures. Geochimica et Cosmochimica Acta, **50**: 1147–1150.

Schönherr, C., Reuning, L., Hallenberger, M., Lüders, V., Lemmens, L., Biehl, B.C., Lewin, A., Leupold, M., Wimmers, K., Strohmenger, C.J., 2018. Dedolomitization: review and case study of uncommon mesogenetic formation conditions Earth-Science Reviews, **185**: 780–805.

Searl, A., 1994. Discontinuous solid solution in Ca-rich dolomites: the evidence and implications for the interpretation of dolomite petrographic and geochemical data. IAS Special Publications, **21**: 361–376.

Smith, D.B., 1981. Bryozoan–algal patch-reefs in the Upper Permian Lower Magnesian Limestone of Yorkshire, north- east England. SEPM Special Publication, **30**: 187–202.

Swart, P.K., 2015. The geochemistry of carbonate diagenesis: the past, present and future. Sedimentology, **62**: 1233–1304.

Usdowski, E., 1994. Synthesis of dolomite and geochemical implications. IAS Special Publications, **21**: 345–360.

Vahrenkamp, V.C., Swart, P.K., 1994. Late Cenozoic dolomites of the Bahamas: metastable analogues for the genesis of ancient platform dolomites. IAS Special Publications, **21**: 133–153.

Vasconcelos, C., McKenzie, J.A., Bernasconi, S., Grujic, D., Tien, A.J., 1995. Microbial mediation as a possible mechanism for natural dolomite formation at low temperatures. Nature, **377**: 220–222.

Veizer, J., 1983. Chemical diagenesis of carbonates: theory and trace element technique. SEPM Short Course, **10**: 3-1–3-100.

Warren, J., 2000. Dolomite: occurrence, evolution and economically important associations. Earth-Science Reviews, **52**: 1–81.

Weber, J.N., Raup, D.M., 1968. Comparison of C^{13}/C^{12} and O^{18}/O^{16} in skeletal calcite of recent and fossil echinoids. Journal of Paleontology, **42**: 37–50.

Wilson, E.N., Hardie, L.A., Phillips, O.M., 1990. Dolomitization front geometry, fluid flow pattern, and the origin of massive dolomite: the Triassic Latemar buildup, northern Italy. American Journal of Science, **290**: 741–796.

Zhang, F., Xu, H., Konishi, H., Roden, E.E., 2010. A relationship between d104 value and composition in the calcite-disordered dolomite solid-solution series. American Mineralogist, **95**: 1650–1656.

Zhang, F., Xu, H., Konishi, H., Shelobolina, E.S., Roden, E.E., 2012a. Polysaccharide-catalyzed nucleation and growth of disordered dolomite: a potential precursor of sedimentary dolomite. American Mineralogist, **97**: 556–567.

Zhang, F., Xu, H., Konishi, H., Kemp, J.M., Roden, E.E., Shen, Z., 2012b. Dissolved sulfide-catalyzed precipitation of disordered dolomite: implications for the formation mechanism of sedimentary dolomite. Geochimica et Cosmochimica Acta, **97**: 148–165.